Tunable Magnetic and Dielectric Properties of $BiFeO_3$ Nanoparticles – Effect of Lanthanum doping

Attia Awan[1)], Saira Riaz[2)], *Adeela Nairan[3)], YB Xu[4)] and Shahzad Naseem[5)]

[1), 2), 3), 5)] *Centre of Excellence in Solid State Physics, University of Punjab, Lahore, Pakistan*
[4)] *Department of Electronics, University of York, UK*
[2)] saira.cssp@pu.edu.pk

ABSTRACT

$BiFeO_3$ is a promising future candidate since it exhibits room temperature antiferromagnetic and ferroelectric properties. However, $BiFeO_3$ suffers from some drawbacks including weak magnetic behavior, inhomogeneity in spin structure and large leakage current. In order to overcome these problems, Lanthanum (La) doped $BiFeO_3$ i.e. $Bi_{1-x}La_xFeO_3$ (where, x=0.1, 0.3, 0.5) NPs are prepared by sol-gel method. NPs show phase pure rhombohedrally distorted perovskite structure of $BiFeO_3$. Dielectric constant remains constant in low frequency region and increases as high frequencies showing anomalous behavior. Tangent loss decreases as frequency increases and becomes constant at high frequencies showing normal dispersion behavior for all concentrations. Dispersion in tangent loss occurs due to the time required by the carriers to get aligned in the direction of field. Decrease in grain size leads to increase in number of grain boundaries hindering the hopping process between the different states and grains thus resulting in accumulation of cations at the grain boundaries, thus affecting the dielectric constant. Magnetic properties show ferromagnetic behavior as opposed to antiferromagnetic nature of bulk $BiFeO_3$. Ferromagnetic behavior arises due to suppression of spiral spin structure with La doping. Increase in magnetization is observed as dopant concentration is increased to 0.3.

1. INTRODUCTION

Pierre Curie gave the idea that crystalline materials can exhibit simultaneous presence of ferroelectric and ferromagnetic orders. After the discovery of ferroelectric switching phenomenon in 1920 by Valasek there were discoveries related to magnetoelectric properties based materials like nickel. Unfortunately, the idea did not proceed. The main break through was provided by Dzyaloshinskii who theoretically predicted magnetoelectricity in Cr_2O_3 followed by experimental discovery by Astrov (Catalan and Scott 2009). But Cr_2O_3 is antiferromagnetic and paraelectric thus limiting

its applications. Work on boracites provided another major breakthrough for ferromagnetic ferroelectrics but these materials only exhibited magnetoelectric effect at exceptionally low temperature (Catalan and Scott 2009). The next advancement in this field was provided by Smolenskii's group with the study of bismuth ferrite that can exhibit ferroelectric and ferromagnetic properties simultaneously at room temperature along with magnetoelectric coupling between them (Catalan and Scott 2009, Quan et al. 2016, Gowrishankar et al. 2016).

At room temperature bismuth ferrite (bismuth iron oxide, $BiFeO_3$) possess rhombohedral structure belonging to R3c space group. This perovskite form of unit cell exhibits lattice parameter a = 3.965Å and α= 89.3-89.48˚. Ferroelectric polarization is present in the direction of [111] pseudo cubic axes. Another convention to describe the unit cell is to consider the hexagonal crystal system. In hexagonal crystal system $[001]_{hexagonal}$ is parallel to $[111]_{pseudocubic}$ and lattice parameters are a =5.58Å and c = 13.90Å. At ~825˚C transition from rhombohedrally distorted perovskite structure to high temperature β-phase is observed along with volume contraction (Tu et al. 2016, Jangid et al. 2012). However, preparation of $BiFeO_3$ is complex due to volatility of its reactants and narrow temperature range for $BiFeO_3$ phase formation. In addition, high leakage current arises from presence of oxygen vacancies and mixed valance state of iron cations. In addition, $BiFeO_3$ exhibits G-type antiferromagnetic behavior with cycloidal spin structure of 62nm (Tu et al. 2016, Jangid et al. 2012).

For improving dielectric and magnetic properties of $BiFeO_3$ various strategies have been proposed including size reduction and doping. Amongst various dopants lanthanum (La^{3+}) reduces the presence of oxygen vacancies as a results of which it stabilizes the oxygen octahedral thus enhancing the ferroelectric and insulating properties. In addition, it suppresses inhomogeneity in the spin structure thus leading to better magnetic properties as compared to undoped $BiFeO_3$ (Kumar et al. 2015, Riaz et al. 2014, Yao et al. 2015, Majid et al. 2015).

We here report sol-gel synthesis of La doped $BiFeO_3$ ($Bi_{1-x}La_xFeO_3$) nanoparticles with variation in dopant concentration (x) as 0.1, 0.3 and 0.5. Changes in magnetic and dielectric behaviors have been correlated with dopant concentration.

2. EXPERIMENTAL DETAILS

Materials used: Analytical grade bismuth nitrate $Bi(NO_3)_3.5H_2O$, iron nitrate $Fe(NO_3)_3.9H_2O$, lanthanum nitrate $La(NO_3)_3.6H_2O$ and ethylene glycol were used without purification.

Preparation Method: $BiFeO_3$ sol was prepared using non vacuum simple and application-oriented sol gel route. Three separate solutions were prepared by dissolving bismuth nitrate, iron nitrate and lanthanum nitrate in ethylene glycol, mixed together and heat-treated at 60^oC with constant stirring in order to obtain a stable sol. A brownish black powder was obtained when heated for two hours. Lanthanum doped bismuth iron oxide nanoparticles with variation in concentration (x=0.1, 0.3, 0.5) were characterized using Bruker D8 Advance X-ray diffractometer (XRD), Lakeshore's 7407 Vibrating sample magnetometer (VSM) and 6500B Precision impedance analyzer.

3. RESULTS AND DISCUSSION

Fig. 1 shows XRD plots for La doped bismuth iron oxide nanoparticles. Splitting of peaks matching with planes (110) and (104) indicate formation of $BiFeO_3$ phase. No peaks matching to bismuth rich or bismuth deficient phases were observed. This indicates that lanthanum doping is effective in stabilizing $BiFeO_3$ nanoparticles. Crystallinity of nanoparticles, indicated by intensities of diffraction peaks, increases as dopant concentration was raised from 0.1 to 0.3. With increase in dopant concentration to 0.5, intensity of diffraction peaks decreased indicating decrease in crystallinity of nanoparticles. Possibility that lanthanum atoms occupy interstitial sites increases at high dopant concentration. This leads to destruction in crystalline order (Riaz et al. 2015). Position of diffraction peaks moves to high angles with increase in dopant concentration. This shift of peak positions is attributed to smaller ionic radii of La^{3+} (1.16Å) as compared to Bi^{3+} cations (1.17Å). This results in reduction in lattice parameters and unit cell volume (Table 1).

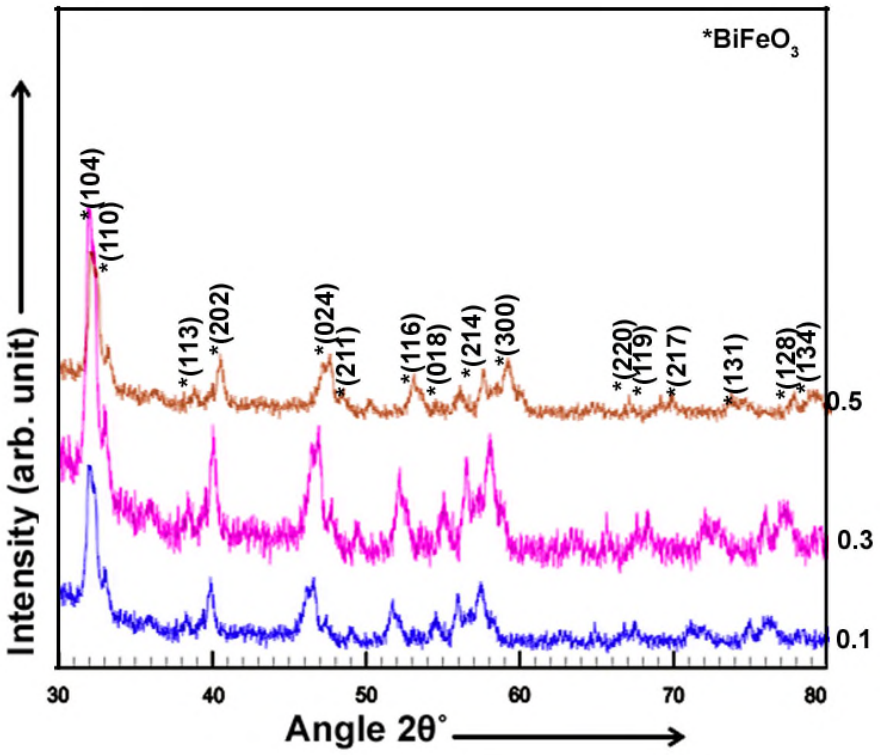

Fig. 1 XRD patterns for La doped $BiFeO_3$ nanoparticles

Tolerance factor was determined using Eq. 1.

$$Tolerance.Factor = \frac{(R_A + R_o)}{\sqrt{2}(R_B + R_o)} \quad (1)$$

Where, R_A is ionic radius of A-site atom, R_B is ionic radius of B site atom, and R_o is ionic radius of oxygen ions. Tolerance factor is given in table 1. It can be seen that tolerance factor decreases from 0.888292 to 0.886909 as dopant concentration was increased. This decrease in tolerance factor is indicative of reduction in Fe-O bond angle as the result of which stiffness in La^{3+}-O^{2-} and Bi^{3+}-O^{2-} bond increases. This results in increased distortion in $BiFeO_3$ lattice (Dhir et al. 2014).

Table 1 Lattice parameters, unit cell volume and tolerance factor for La doped $BiFeO_3$ nanoparticles

Dopant concentration (x)	Lattice parameters (Å)		Unit Cell volume ($Å^3$)	Tolerance factor
	a	c		
0.1	5.500	13.98	366.2271	0.888292
0.3	5.495	13.975	365.4308	0.887601
0.5	5.489	13.768	359.2322	0.886909

Crystallite size (Cullity 1956) and dislocation density (Kumar et al. 2011) were calculated using Eqs. 2-3, respectively.

$$t = \frac{0.9\lambda}{B\cos\theta} \quad (2)$$

$$\delta = \frac{1}{t^2} \quad (3)$$

Where, θ is the diffraction angle, λ is the wavelength (1.5406Å) and B is Full Width at Half Maximum. Increase in crystallite size (Fig. 2) from 16.59nm to 19.23nm was observed with increase in dopant concentration from 0.1 to 0.3. In sol-gel synthesis, crystallite size strongly depends on nucleation step. Adding La^{3+} cations in $BiFeO_3$ results in localized heating around the ions due to smaller ionic radius of La^{3+} ion as compared to Bi^{3+}. As a result, temperature gradient is created in the solution. This helps in Ostwald ripening mechanism thus increasing the crystallite size (Riaz et al. 2015). At dopant concentration of 0.5 the decrease in crystallite size is associated with occupation of La^{3+} cations on interstitial sites or grain boundaries.

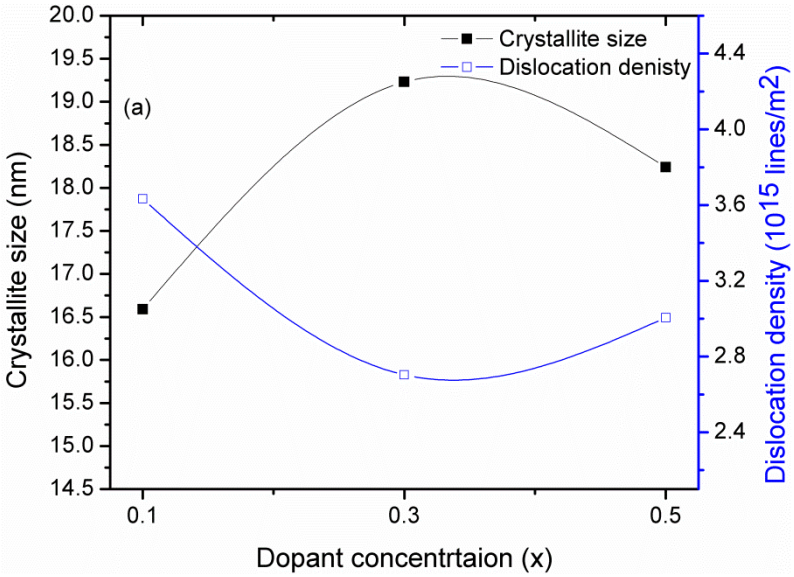

Fig. 2 Crystallite size and dislocation density plotted as a function of dopant concentration

Fig. 3 shows M-H curves for La doped $BiFeO_3$ nanoparticles. La doped $BiFeO_3$ nanoparticles show ferromagnetic behavior. Bulk $BiFeO_3$ is known to have antiferromagnetic properties. Modifications in magnetic properties take place due to presence of some energy barrier. Phenomena responsible for this energy barrier include magnetostatic length and crystalline anisotropy. These length scales determine that the distance over the magnetic moments will deviate significantly. These length scales are also representative of domain wall width of specimen. This length scale for $BiFeO_3$ is reported to be 62nm (Shah et al. 2014a,b). So if the grain size falls below this limit ferromagnetic behavior arises in otherwise antiferromagnetic material due to suppression of helical spin structure. It can be seen in Fig. 3 that there is a conversion from weak ferromagnetic to strong magnetic behavior. Lattice distortion increases as La^{3+} cations replace Bi^{3+} cations. This results in variation in canting angle that is associated with Fe-O-Fe bond supported by decrease in tolerance factor (table 1). This increased distortion results in transition from weak magnetic behavior to strong magnetic behavior. In addition as La^{3+} replace Bi^{3+} cations magnetic sublattices associated with La and Fe are created that are ferromagnetically coupled (Shah et al. 2014a,b). This also results in enhanced magnetization with increase in dopant concentration.

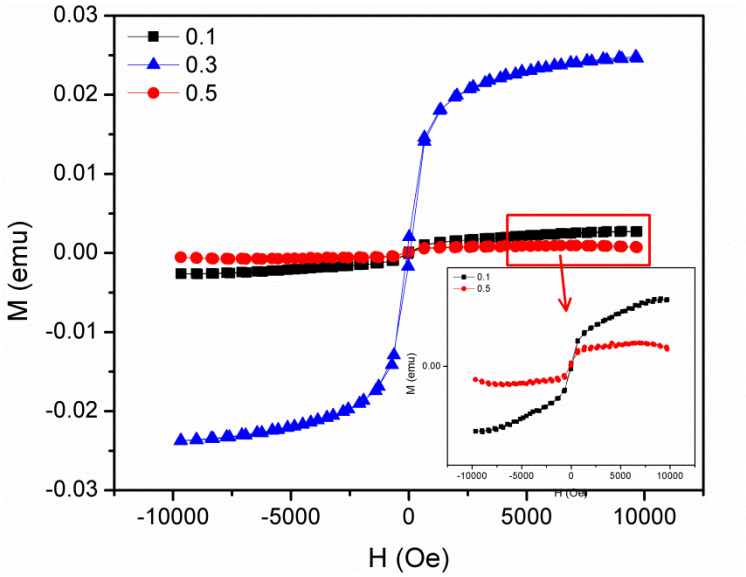

Fig. 3 M-H curves for La doped $BiFeO_3$ nanoparticles

Fig. 4 shows dielectric constant and tangent loss for bismuth iron oxide nanoparticles. Dielectric constant remains constant in low frequency region. As frequency of applied field increased increase in dielectric constant was observed. This increase of dielectric constant at high frequencies is attributed to resonance effect. This effect arises when hopping frequency of ions is well matched with the applied field frequency (Yang et al. 2010). On the other hand, decrease in tangent loss was observed at low frequencies only. This behavior of tangent loss is in accordance with Maxwell Wagner's two layered model. Polycrystalline material consists of 1) Grains (high conductivity); 2) Grain boundaries (High resistivity). Grains have high conductivity and role of grains dominate at high frequencies (Riaz et al. 2014a,b, Riaz et al. 2015). Grain boundaries are less conducting and their role dominates at low frequencies. This results in normal dispersion behavior of tangent loss (Fig. 4(b)). It can be seen from Fig. 4(a) and (b) that dielectric constant increases from 70 (log f = 5.0) to 140 (log f = 5.0) as dopant concentration was increased from 0.1 to 0.3. Dielectric constant strongly depends on grain size. Increase in crystallite size leads to increase in probability of the formation of 180˚ domains that offers high polarization. This increases the dielectric constant. In addition, La^{3+}-O^{2-} ions offers high stability as compared to Bi^{3+}-O^{2-} ions. Thus, number of oxygen vacancies decreases with increase in dopant concentration thus resulting in increase in dielectric constant.

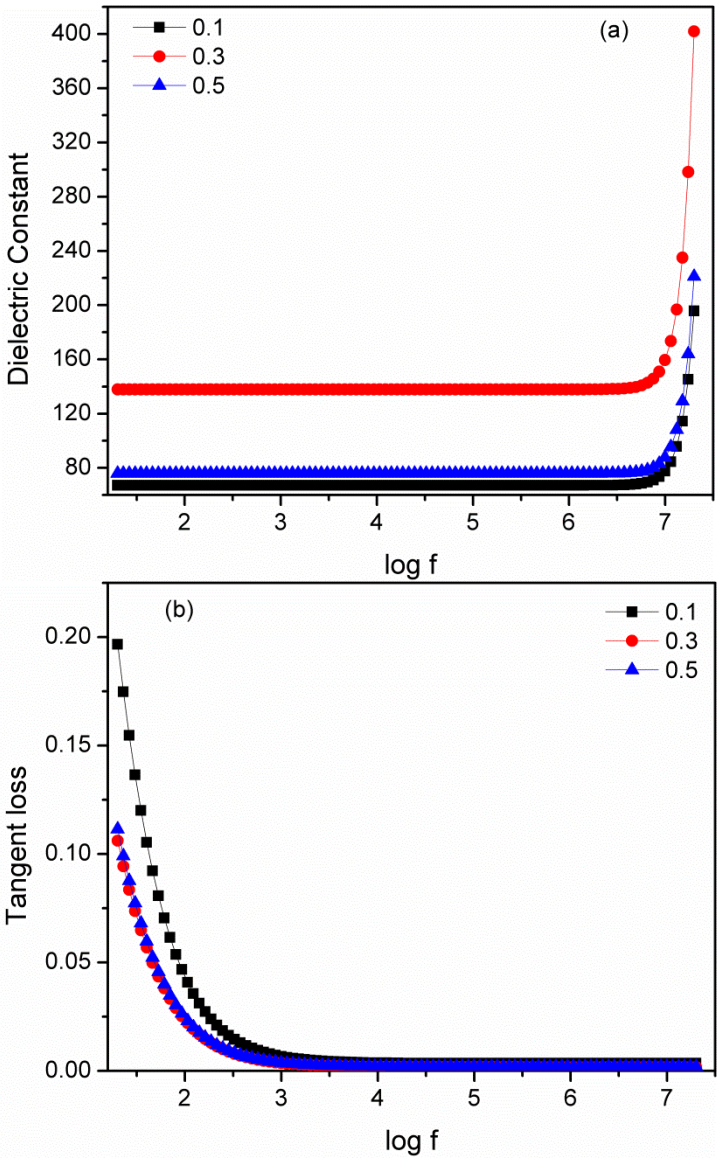

Fig. 4 (a) Dielectric constant (b) tangent loss for La doped $BiFeO_3$ nanoparticles

4. CONCLUSIONS

La doped $BiFeO_3$ nanoparticles have been successfully synthesized using non vacuum sol gel technique. Dopant concentration (i.e. x in $Bi_{1-x}La_xFeO_3$) was varied as 0.1, 0.3 and 0.5. X-ray diffraction results confirmed the formation of phase pure $BiFeO_3$. Crystallite size increased and dislocation density decreased at dopant concentration 0.3. La doped $BiFeO_3$ nanoparticles prepared using 0.3 dopant concentration resulted in strong ferromagnetic behavior. Ferromagnetism in $BiFeO_3$ arises due to linearity in spin structure. Dielectric constant showed anomalous dispersion while normal dispersion behavior was observed for tangent loss data. Dielectric constant increased from 70 (log f = 5.0) to 140 (log f = 5.0) and tangent loss decreased with increase in dopant concentration from 0.1 to 0.3.

REFERENCES

Chern, J.C., Yang, H.J. and Chen, H.W. (1992), "Behavior of steel fiber reinforced concrete in multi axial loading", *ACI Mat. J.,* **89**(1), 32-40.

Cullity, B.D. (1956), "Elements of x-ray diffraction," Addison Wesley Publishing Company, USA.

Dhir, G., Uniyal, P. and Verma, N.K. (2014), "Effect of Particle Size on Magnetic and Dielectric Properties of Nanoscale Dy-Doped $BiFeO_3$," *J. Supercond. Nov. Magn.*, **27**, 1569-1577.

Gowrishankar, M., Babu, D.R. and Saravanan, P. (2016), "Room temperature multiferroism in La and Ti co-substituted BiFeO3 nanoparticles," *Mater. Lett.*, **171**, 34–37.

Jangid, S., Barbar, S.K., Bala, I. and Roy, M. (2012) "Structural, thermal, electrical and magnetic properties of pure and 50% La doped $BiFeO_3$ ceramics," *Phys. B*, **407**, 3694–3699

Kumar, N., Sharma, V., Parihar, U., Sachdeva, R., Padha, N. and Panchal, C.J. (2011) "Structure, optical and electrical characterization of tin selenide thin films deposited at room temperature using thermal evaporation method," *J. Nano- Electron. Phys.*, **3**, 117-126

Kumar, P., Panda, C. and Kar, M. (2015), "Effect of rhombohedral to orthorhombic transition on magnetic and dielectric properties of La and Ti co-substituted $BiFeO_3$," *Smart Mater. Struct*., **24**, 045028

Majid, F., Riaz, S. and Naseem, S. (2015), "Microwave-assisted sol–gel synthesis of $BiFeO_3$ nanoparticles," *J. Sol-Gel Sci. Technol.* **74**, 329-339.

Quan, C., Han, Y., Gao, N., Mao, W., Zhang, J., Yang, J., Lia, X. and Huang, W. (2016), "Comparative studies of pure, Ca-doped, Co-doped and co-doped $BiFeO_3$ nanoparticles," *Ceram. Int.*, **42**, 537–544.

Riaz, S., Majid, F., Shah, S.M.H. and Naseem, S. (2014a), "Enhanced magnetic and structural properties of Ca doped BiFeO3 thin films," *Indian J. Phys.* **88**, 1037–1044.

Riaz, S., Shah, S.M.H., Akbar, A., Atiq, S. and Naseem, S. (2015), "Effect of Mn doping on structural, dielectric and magnetic properties of $BiFeO_3$ thin films," *J. Sol-Gel Sci. Technol.* **74**, 310-319.

Riaz, S., Shah, S.M.H., Akbar, A., Kayani, Z.N. and Naseem, S. (2014b) "Effect of Bi/Fe Ratio on the Structural and Magnetic Properties of $BiFeO_3$ Thin Films by Sol-Gel," *IEEE Trans. Magn.* **50**, 2201304.

Shah, S.M.H, Akbar, A., Riaz, S., Atiq, S. and Naseem, S. (2014a), "Magnetic, Structural, and Dielectric Properties of $Bi_{1-x}K_xFeO_3$ Thin Films Using Sol-Gel," *IEEE Trans. Magn.* **50**, 2201004.

Shah, S.M.H., Riaz, S., Akbar, A., Atiq, S. and Naseem, S. (2014b), "Effect of Solvents on the Ferromagnetic Behavior of Undoped BiFeO3 Prepared by Sol-Gel," *IEEE Trans. Magn*. **50**, 2200904.

Tu, C.S., Chen, C.S., Chen, P.Y., Xu, Z.R., Idzerda, Y.U., Schmidt, V.H., Lyu, M.Q., Chan, T.S. andLin, C.Y. (2016), "Raman Vibrations, Domain Structures, and Photovoltaic Effects in A-Site La-Modified BiFeO3 Multiferroic Ceramics," *J. Am. Ceram. Soc.,* **99**, 674–681.

Yang, C., Jiang, J.S., Qian, F.Z., Jiang, D.M., Wang, C.M. and Zhang, W.G. (2010), "Effect of Ba doping on magnetic and dielectric properties of nanocrystalline $BiFeO_3$ at room temperature," *J. Alloy Compd.,* **507**, 29–32.

Yao, Q.R., Cai, J., Zhou, H.Y., Rao, G.H., Wang, Z.M. and Deng, J.Q. (2015), "Influence of La-doping on structure and magnetic behaviors in BiFeO3," *J. Alloy Compd.*, **633**, 170–173